Phase transition kinetics in colloid-polymer mixtures at triple coexistence: Kinetic maps from free-energy landscapes

F. Renth, W. C. K. Poon, and R. M. L. Evans
Department of Physics and Astronomy, The University of Edinburgh, Mayfield Road, Edinburgh, EH9 3JZ, Scotland
(Received 26 March 2001; published 30 August 2001)

We report a detailed experimental study of the kinetics of separation into coexisting gas, liquid, and crystal phases in a colloid-polymer mixture. Distinct kinetic regimes are identified, and interpreted in terms of the underlying ''free-energy landscape'' of the system.

DOI: 10.1103/PhysRevE.64.031402 PACS number(s): 82.70.Dd, 64.60.My, 64.75.+g

I. INTRODUCTION

Gibbs and Boltzmann gave us a recipe for calculating the *equilibrium* phase behavior of an N-particle system with potential energy $U(\vec{r}_N)$ at temperature T and confined to volume V—minimize the Helmholtz free energy

$$F = Vf(\rho,T) = -k_B T \ln \int e^{-U(\vec{r}_N)/k_B T} d\vec{r}_N , \qquad (1)$$

where $\rho = N/V$ and f is the free-energy density. While plenty remains to be explored in equilibrium phase behavior, especially in novel materials, the basic theory must be considered well established. This recipe, however, gives no information on *processes*—how does a system in thermodynamic equilibrium respond if the conditions under which it is held are changed suddenly (''quenched'')? Answering this question is an important challenge in condensed matter and statistical physics. It also pays rich practical dividends: many industrial products are in metastable states. How they get into such states in the first place may, for example, control the mesoscopic texture (as in alloys) and therefore mechanical properties. How long they take to get out of metastability often controls the shelf life (as in salad dressing).

Theoretically, computationally, and experimentally, it is hard to tackle phase transition kinetics, so that our understanding of it lags considerably behind that of equilibrium phase behavior. Theoretically, phenomenological models are common [1]. ''Model B,'' for example, gives the following equation of motion for a conserved order parameter [e.g., the time-dependent density profile $\rho(\vec{r},t)$]:

$$\frac{\partial \rho}{\partial t} = \vec{\nabla} \cdot \left[M(\rho) \vec{\nabla} \left(\frac{\partial f(\rho)}{\partial \rho} - \kappa \nabla^2 \rho \right) \right], \qquad (2)$$

where $f(\rho)$ is the free-energy density already introduced in Eq. (1). Apart from its analytical intractability, this equation contains phenomenological constants such as the order-parameter mobility M and the curvature coefficient κ, which are generally unknown. Even so, advances have been made [2], e.g., in classifying dynamics into universality classes, but progress is slow due to intrinsic mathematical difficulties. Such coarse-grained models are often also the starting point of computational approaches, because simulations containing more realistic molecular-level details will take prohibitively long to reach interesting time and length scales.

Time and length scales also present experimental problems. A homogeneous substance phase separating into (say) two coexisting phases develops structure on length and time scales ranging from the microscopic (picosecond and nanometer) to the macroscopic (seconds to years and centimeters upward). The initial fast times and small lengths are intrinsically hard to probe. The later stages may not be accessible on a human time scale. In this context, complex fluids, liquids in which there are mesoscopic structural elements such as suspended particles, self-assembled surfactant micelles, or polymer coils, often emerge as ideal candidates for detailed studies of phase transition kinetics. Firstly, the upper end of the mesoscopic length scale, ~ 1 μm, is comparable to the wavelength of light, so that direct imaging using optical microscopy can be used to access even the smallest relevant length scales. Secondly, the intrinsic, entropy-controlled relaxation times of complex fluids are long, typically 10^{-3} s upwards. These are, of course, modified by specific interactions. But attractions much more than $10k_BT$ are uncommon. The end result is that the characteristic times over which kinetics evolve are likely to be in the range 1 ms to 1 year. Finally, complex fluids are ''soft.'' Their small elastic moduli mean that they can be put in highly reproducible initial metastable states by simple shear. For these reasons, complex fluids are emerging as ideal laboratories for studying all kinds of nonequilibrium phenomena, including phase transition kinetics [3].

In this and a companion paper [4], we report a detailed study of a well-characterized complex fluid—a mixture of nearly-hard-sphere colloids and nonadsorbing, random coil polymers that shows up to three equilibrium phases, (colloidal) gas, liquid, and crystal. Samples with the right composition may show coexistence of all three phases. We study the pathways whereby such samples, after homogenization, separate into macroscopically coexisting colloidal gas, liquid, and crystal regions. We find the existence of distinct kinetic regimes, and make sense of this finding by investigating the ''free-energy landscape'' of the system. Our approach to understanding kinetics should be generically applicable, especially in, but not confined to, soft systems. This is also one of the first in-depth studies of the kinetics of *three*-phase separation—the vast majority of existing studies deal with separation into two coexisting phases.

In this paper we review the physics of colloid-polymer mixtures and describe briefly how the free-energy landscape gives rise to kinetic regimes. After introducing our experi-

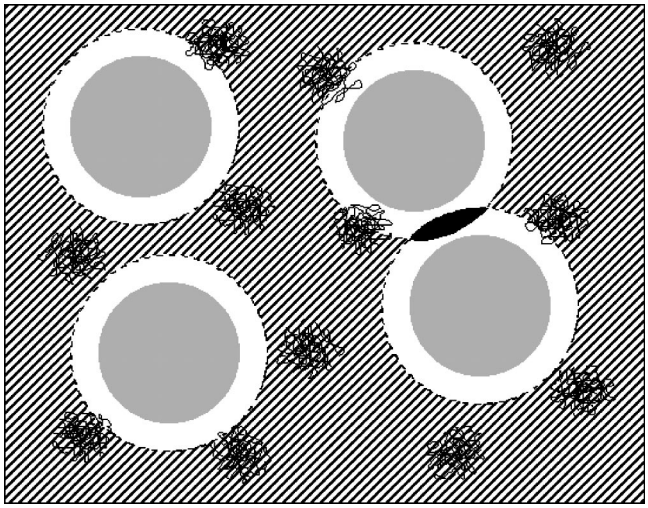

FIG. 1. Schematic illustration of depletion and free volume. Each colloidal particle (gray) is surrounded by a depletion zone (white) from which the centers of the random coil polymers (black coils) are excluded. The free volume V_{free} available to the centers of the polymers is hatched. If the depletion zones of two colloids overlap (black), V_{free} increases.

mental system and methodology, we proceed to report and interpret our experimental findings. Details of the theory, as well as numerics confirming the validity of its various assumptions, are given in a companion paper [4]. A concise presentation of our findings has been given before [5]. There is also a short pedagogical account on relating free-energy landscapes to kinetics [6].

II. COLLOID-POLYMER MIXTURES

The addition of a nonadsorbing polymer to a suspension of colloidal particles alters its phase behavior. The simplest model for the effect of nonadsorbing polymers (radius of gyration r_g) on colloids (radius R) was due to Asakura and Oosawa [7], Fig. 1. Consider the simplest case, that of *hard-sphere* colloids. Polymer segments are depleted from a layer of thickness $\sim r_g$ around each particle. The overlap of the ''depletion layers'' of two nearby particles creates additional free volume for the polymer, thus lowering the free energy. This can be modeled as an effective interparticle ''depletion attraction''

$$U_{\mathrm{dep}}(r) = -\Pi_{\mathrm{P}} V_{\mathrm{ov}}(r) = -(a_{\mathrm{P}} k_B T) V_{\mathrm{ov}}(r), \tag{3}$$

where Π_{P} is the osmotic pressure of the polymer and $V_{\mathrm{ov}}(r)$ is the (interparticle-distance-dependent) volume of overlap of neighboring depletion layers. This pertains to ideal polymers at activity a_{P} (which equals the polymer number density in the free volume, see Fig. 1), which is related to the polymer chemical potential μ_{P} (and its de Broglie thermal wavelength Λ_{P}) by

$$a_{\mathrm{P}} = \Lambda_{\mathrm{P}}^{-3} e^{\mu_{\mathrm{P}}/k_B T}. \tag{4}$$

The topology of the colloid-polymer phase diagram depends on the size ratio $\xi = r_g/R$. When ξ is big enough, the phase diagram shows colloidal gas, liquid, and crystal re-

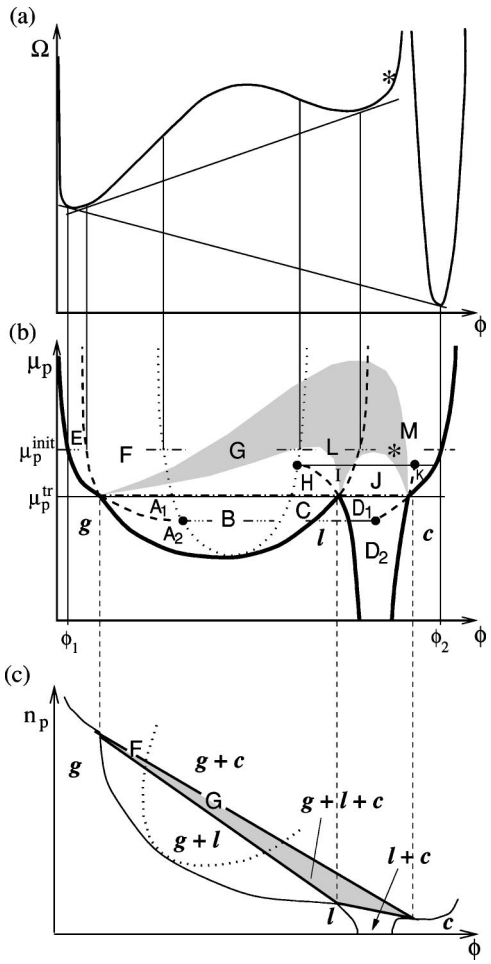

FIG. 2. (a) Schematic semigrand potential density as a function of colloid volume fraction $\Omega(\phi)$—the free-energy landscape for the polymer chemical potential μ_p^{init}. The fluid (crystal) branch displays double (single) minima. The lower and upper common tangents give, respectively, at their cotangency points, the densities of coexisting stable and metastable phases at $\mu_{\mathrm{p}} = \mu_{\mathrm{p}}^{\mathrm{init}}$. The spinodal region, $\partial^2\Omega/\partial\phi^2 < 0$, is between the middle two vertical lines. (b) The schematic (ϕ, μ_{p}) phase diagram. As μ_{p} is varied, $\Omega(\phi)$ changes shape. The cotangency points of the lowest common tangent traces out the equilibrium phase boundaries (bold curves). Other pairs of cotangency points (dashed) and the spinodal points (dotted) divide the phase diagram into kinetic regions A–M. Three-phase coexistence occurs at $\mu_{\mathrm{p}} = \mu_{\mathrm{p}}^{\mathrm{tr}}$. Metastable, homogeneous samples in the gray area separate into three phases. (c) The schematic (ϕ, n_{p}) phase diagram. Samples within the triple triangle separate into coexisting colloidal gas (g), liquid (l), and crystal (c). This triangle maps onto the gray region in (b). The gas-liquid spinodal (dotted) and kinetic regions F and G are sketched in.

gions [8,9]. If we use as variables the colloid volume fraction ϕ and the polymer chemical potential μ_{P} (which is, up to a constant, $k_B T \ln a_{\mathrm{P}}$), then the phase diagram is similar to (in fact an upside-down version of) that of a simple substance in the density-temperature plane, Fig. 2(b). Thus there are regions where homogeneous colloidal gas, liquid, and crystal phases are thermodynamically stable. In other regions, the lowest free energy is obtained with heterogeneous, two-phase coexistence, whether it be of gas-liquid, liquid-crystal,

or gas-crystal forms. At one particular polymer chemical potential, μ_P^{tr}, the triple coexistence of gas, liquid, and crystal phases is obtained. In this representation, tie lines in two-phase regions, connecting the state points of coexisting phases, are horizontal, expressing the equality of the polymer chemical potential in the two phases.

The polymer activity a_P is not directly controllable experimentally. The actual variable tuned in the laboratory is the polymer *concentration*, as measured by, e.g., n_P, the number density of polymer coils in the total sample volume. The phase diagram in the (ϕ, n_P) plane is shown schematically in Fig. 2(c). Tie lines in two-phase regions are now oblique, expressing the obvious fact that there is less polymer in a phase denser in colloids. More significantly for our purposes, the triple-coexistence *line* in the (ϕ, μ_P) representation now becomes a triple *triangle*. Any homogeneous mixture with composition within this triple triangle will eventually phase separate into coexisting colloidal gas, liquid, and crystal phases with compositions given by the vertices of the triangle.

Note that the triple triangle in Fig. 2(c) maps onto a ''bat''-shape region in the representation shown in Fig. 2(b); this region is *above* the triple line except at three points. This reflects the fact that in a *homogeneous* sample with composition within the triple triangle, the polymer chemical potential is *higher* than μ_P^{tr}, and only drops to this value when three-phase separation is complete—the sample has become heterogeneous, and consists of gas, liquid, and crystal regions in thermal equilibrium. Shaking such a sample to homogenize it therefore corresponds to a ''chemical-potential quench.''

Before turning to consider the kinetics of the three-phase separation process, which is the main thrust of this and the following paper, we briefly review how to calculate the phase diagrams of colloid-polymer mixtures. The basic quantity is the Helmholtz free energy of N_C colloids and N_P polymers confined to total volume V. Within a mean-field van der Waals framework and for ideal polymers [8], the free energy is separable,

$$F_{total}(N_C, N_P, V) = F_C(N_C, V) + F_P(N_P, V_{free}). \tag{5}$$

Here, $F_C(N_C, V) \equiv F_C(\phi)$ is the Helmholtz free energy of pure colloids at volume fraction ϕ *unperturbed* by polymers, and $F_P(N_P, V)$ is the Helmholtz free energy of N_P ideal polymer coils confined to the free volume. That is to say, the polymer has no effect on the colloids, and the only effect of the colloid on the polymer is to confine the molecules into the free volume, V_{free}, Fig. 1, which in this approximation is related to the total sample volume V by a number that is (at fixed ξ) simply ϕ dependent,

$$V_{free} = \alpha(\phi) V. \tag{6}$$

Minimizing F_{total} with respect to ϕ and $n_P = N_P/V$ gives a phase diagram in the representation shown in Fig. 2(c).

Alternatively, we can transform from the (ϕ, n_P) (canonical) ensemble into a semigrand ensemble, (ϕ, a_P), in which the polymer chemical potential, or, equivalently, the polymer activity, is the polymeric variable. The appropriate semigrand potential is

$$V\Omega(\phi, a_P) = F(\phi, n_P) - N_P \mu_P = F_C(\phi) - (a_P k_B T) V_{free}, \tag{7}$$

where the last equality is valid for ideal polymers. Minimizing $\Omega(\phi, a_P)$ with respect to ϕ gives a phase diagram in the representation shown in Fig. 2(b).

The minimization of the semigrand potential can be discussed geometrically by plotting the semigrand potential *density* Ω as a function of the colloid volume fraction ϕ, giving the ''free-energy landscape'' of the system. Depending on the value of a_P, the fluid branch of $\Omega(\phi, a_P)$ has either one or two minima, while the crystal branch has a single minimum for the values of ξ of interest in this work. Consider the resulting plot, the free-energy landscape, for the particular case shown in Fig. 2(a). Minimization is done geometrically by drawing the lowest common tangent, with points of tangency at ϕ_1 and ϕ_2. Homogeneous samples with $\phi < \phi_1$ or $\phi > \phi_2$ are stable as single-phase colloidal gas or crystal, respectively. A sample with average density $\phi_1 < \phi < \phi_2$ will separate into coexisting colloidal gas (density ϕ_1) and crystal (density ϕ_2). The metastable second (''liquid'') minimum in the fluid branch is irrelevant for equilibrium phase behavior. It does, however, control the phase transition kinetics.

We turn now to summarize a theoretical framework for considering the kinetic influence of metastable minima in the free-energy landscape. This framework predicts that the phase diagram is divided into distinct kinetic regions. We then present a detailed series of experiments on a model colloid-polymer mixture in which such kinetic regions are indeed found.

III. FREE-ENERGY LANDSCAPE AND KINETICS

In this section we review a procedure for turning an equilibrium phase diagram into a ''kinetic map,'' delineating regions in which distinct kinetic pathways are permitted in phase separation processes. This procedure was first suggested by Cahn [10] in the context of crystallization in vitrified ceramics. Here we extend it to consider phase separation kinetics in colloid-polymer mixtures. Detailed justification is left to the companion paper [4]. Below we motivate and state the results without proof to provide a framework within which to present experimental results.

The Cahn procedure is based on considering the free-energy landscape of the system. Consider a mixture with the kind of free-energy landscape shown in Fig. 2(a), resketched in Fig. 3. The three minima correspond to colloidal gas, liquid, and crystal phases. It can easily be shown that in a homogeneous, metastable sample at density ϕ_a, the free energy (density) available to nucleate an *infinitesimal* amount of a domain at density ϕ_b is given by constructing the tangent (α) to $\Omega(\phi)$ at ϕ_a, and finding the distance between this tangent and $\Omega(\phi)$ at ϕ_b, i.e., the distance $\Delta\Omega$ in Fig. 3. This construction immediately tells us that this sample will *never* commence phase separation by nucleating gas drop-

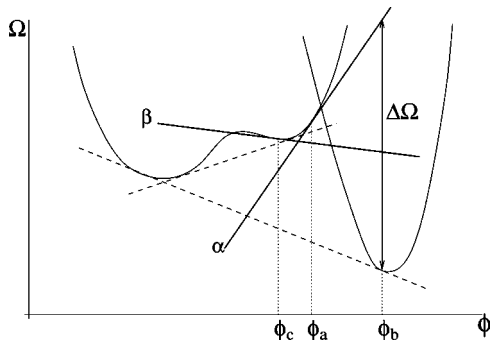

FIG. 3. The ''Cahn'' construction on a free-energy landscape giving the free energy available, $\Delta\Omega$, to create an infinitesimal amount of composition ϕ_b in a metastable phase at composition ϕ_a.

lets, since the tangent α is *below* the gas minimum in the free-energy landscape. This sample can only nucleate crystallites. Moreover, note that no common tangent can be constructed between the crystal and liquid minima—thus no stable interface between any crystallite and the surrounding liquid is possible. Common tangents can, however, be drawn between the crystal and gas minima, and between the gas and liquid minima. Thus, the system will initiate phase separation by nucleating a crystallite that is coated by a layer of gas which coexists in local equilibrium with both the crystallite and the surrounding liquid. By analogy with its concentric layers, we shall refer to such a composite structure as a ''boiled-egg crystal.'' This will deplete the surrounding liquid and rotate the Cahn tangent clockwise until it lies above the gas well, whence nucleation of gas droplets also becomes possible. At the same time, μ_{p} will decrease and approach $\mu_{\mathrm{p}}^{\mathrm{tr}}$, changing the shape of the free-energy landscape. At some point, a liquid-crystal common tangent becomes possible, permitting the nucleation of ''bare'' (i.e., not gas-coated) crystallites.

Changing the density of the homogeneous sample can produce sudden changes in the allowed route to phase separation. Thus, a sample at ϕ_c, Fig. 3, can nucleate the boiled-egg crystallites already discussed as well as gas droplets on their own: the tangent β is above both the gas and the crystal minima. Such changes in allowed phase pathways can also be brought about by shifting the relative positions of the three minima, i.e., by changing μ_{P} of the homogeneous sample. Overall, therefore, this procedure divides the equilibrium phase diagram up into kinetic regions. A moment of thought should suggest that these regions are demarcated by the common tangents between pairs of minima in the free energy landscape, i.e., by metastable continuations of the various equilibrium phase boundaries, and by the gas-liquid spinodal [points of inflection on the fluid branch of $\Omega(\phi)$]. Note that the metastable continuations of the two branches of the liquid-crystal binodal terminate when the liquid branch intersects the gas-liquid spinodal. In terms of the free-energy landscape, this corresponds to the nonexistence of a double tangent between the liquid and crystal minima already described. The resulting kinetic regions are shown schematically in Fig. 2(b).

The free-energy landscape shown in Fig. 2(a) is appropriate for the polymer chemical potential $\mu_{\mathrm{p}}^{\mathrm{init}}$ in Fig. 2(b). The boiled-egg crystal at the first scenario described above corresponds to a sample at position indicated by an asterisk in Figs. 2(a) and 2(b) (cf. ϕ_a in Fig. 3), which is identified as region *M* in a full classification [4]. The scenario described at ϕ_c in Fig. 3, where both gas and boiled-egg crystals can be nucleated, evidently corresponds to the region to the immediate left in Fig. 2(b), i.e., region *L*. At somewhat lower μ_{p}, where a metastable common tangent between liquid and crystal minima becomes possible, then nucleation of bare crystallites (i.e., not coated by a gas layer) is allowed, either on their own, region *J*, or with gas droplets, region *I*. The largest kinetic region is *G*. Here, the homogeneous sample is unstable towards separating into gas and liquid; nucleation of crystallites (bare or coated) is also allowed, although the former is expected to be considerably faster and therefore the first to be observed in experiments, followed by crystal nucleation from the gas or liquid regions.

Other kinetic regions can be similarly described. A compact, graphical notation for doing so is introduced in Sec. IV B of the following paper [4], and the kinetic pathways permitted in regions *A* to *M* are tabulated using this notation in Sec. IV C of that paper.

The boundaries of the kinetic regions *F*, *G*, *I*, *J*, *L*, and *M* shown in Fig. 2(b) intersect the bat-shaped region, and therefore map onto corresponding kinetic regions in the triple triangle in the (ϕ, n_{P}) representation. We provide an indication of this mapping by labeling regimes *F* and *G* in the triple triangle in Fig. 2(c). Other kinetic regimes are found in a comparatively small area towards the liquid and/or crystal end of the triple triangle, and are not indicated individually. Nevertheless, we can infer locations based on Fig. 2(b). For example, reference to the ''bat'' shows that we expect regime *I* behavior in the vicinity of the liquid corner of the triple triangle. Below, we present evidence that distinct kinetic regions do indeed exist within the three-phase triangle, and that the observed kinetic pathways correlate well with the predictions from considering the free-energy landscape.

IV. EXPERIMENT

We studied mixtures of colloidal polymethylmethacrylate (PMMA) spheres and linear polystyrene dispersed in hydrocarbon solvents. The equilibrium phase behavior of this system has been studied extensively before [9]. The PMMA spheres are sterically stabilized by a thin (≈ 10 nm), chemically grafted surface layer of poly-12-hydroxystearic acid (PHSA) [11]. The particle radius was determined using both powder light crystallography [12] and differential interference contrast (DIC) optical microscopy to be $R = 240$ nm. The polydispersity (from static light scattering [13]) was $\sigma = 0.08$. The PMMA spheres were dispersed in cis-decahydronaphthalene (cis-decalin, Aldrich). Previous studies have shown that in cis-decalin, these particles reproduce the hard-sphere phase behavior predicted by computer simulations [14]. Thus, the colloid volume fraction can be cali-

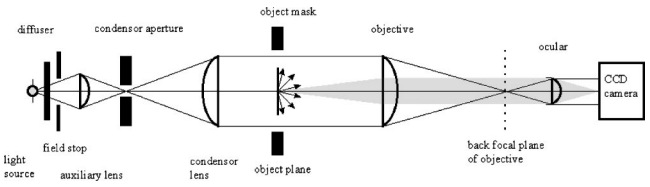

FIG. 4. Schematic illustration of the setup used for time-resolved observation in transmitted light. The components to the left of the sample (''object'') provide collimated white light illumination, while those to the right project the transmitted light image of the sample onto the chip of a CCD camera for digital image grabbing and time-lapsed video recording.

brated relative to the crystallization transition at $\phi = 0.494$ [15,16].

The polymer was polystyrene (PS) with a molecular weight $M_w = 7.3 \times 10^6$ g mol^{-1} and a heterogeneity $M_w/M_n = 1.04$ (Polymer Laboratories Ltd., UK). Its short-time diffusion constant in cis-decalin was measured using dynamic light scattering at the theta temperature $T_\theta = 12.5\,^\circ$C. The radius of gyration r_g^θ was then calculated using the Stokes-Einstein relation and the known relation of r_g and r_H [17] to be 73 ± 4 nm, in excellent agreement with the data of Berry [18]. Finally, the radius at 24.5 °C was calculated (using the results from Flory [19] and Berry [18]) to be $r_g = 88$ nm. At room temperature, deviations from an ideal gas equation of state [as used in Eq. (3)] are negligible for our purposes [20].

Samples were prepared by mixing colloid stock suspension and PS stock solution, and diluted to the desired volume fraction by adding calculated amounts of cis-decalin, using literature values for the densities of PMMA and cis-decalin. Each sample was then homogenized by prolonged tumbling. We determined the equilibrium phase behavior of our system, which has a size ratio $\xi = r_g/R \approx 0.37$, by preparing samples covering a wide range of ϕ and c_p (polymer concentration) in 2 ml glass vials. All samples were inspected visually at regular intervals. Due to the partial refractive index matching (PMMA, $n \approx 1.495$; cis-decalin, $n \approx 1.48$), the samples were sufficiently translucent to identify crystallization and phase boundaries in the bulk easily. Further data points were obtained by careful dilution of existing samples. Solvent evaporation caused insignificant changes in the sample composition over several months.

Samples for kinetic observations were made from colloid-polymer mixtures with known equilibrium phase behavior in standard rectangular optical cuvettes with 2 mm optical path length and 1 cm width (Starna). The majority of observations were performed in transmitted light at $24.5 \pm 0.5\,^\circ$C on an optical bench using a setup shown schematically in Fig. 4. The magnification achieved can be tuned by changing the focal lengths of the various lenses. If the whole width of a sample (1 cm) is imaged, a lateral resolution of ~ 0.3 mm can be achieved [limited by the pixellation of the charge-coupled device (CCD) camera chip]. The depth of focus is 0.5 mm. Images were recorded continuously by time-lapse video as well as by digital frame-grabbing at regular intervals.

In transmitted light, colloidal fluid phases can be distinguished by the image intensity, a gas phase scatters less and therefore appears brighter than a liquid phase. To confirm this identification in complex phase separation scenarios, and to check for the presence of crystallites, frequent observations by eye were also carried out. Crystallites are iridescent to the naked eye, but appear as dark patches in transmitted light images. Video recording at the Bragg angle was also carried out in selected cases in order to monitor crystallite formation. Because of the slightly higher density of the colloidal particles with respect to the solvent, any crystal phase existing at final equilibrium will be at the bottom of the sample, with liquid next and then gas phase on top. Samples were homogenized immediately prior to being transferred to the optical setup.

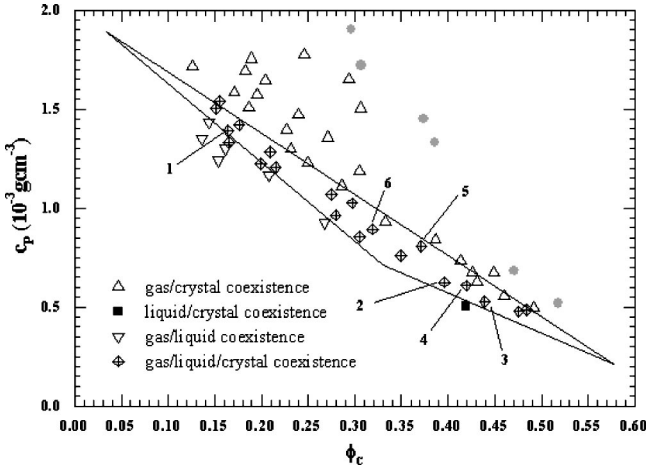

FIG. 5. Experimental phase diagram for a mixture of PMMA colloidal particles ($R = 240$ nm) and linear PS ($M_w = 7.3 \times 10^6$ gmol^{-1}, $r_g = 88$ nm) in cis-decalin at 25 °C. The horizontal axis is the colloid volume fraction ϕ_c and the vertical axis is the polymer concentration c_p. The approximate boundary of the region of triple coexistence is indicated by the triangle. The typical error of sample composition is of the order of the symbol size. Symbols for various types of equilibrium coexistence are explained in the inset. Filled circles stand for nonequilibrium transient gels.

V. RESULTS AND DISCUSSION

A. Equilibrium phase diagram

The experimental phase diagram is shown in Fig. 5. The equilibrium phase behavior of samples within the triangular region is the triple coexistence of colloidal gas, liquid, and crystal, with compositions given by the respective corners of the triangle. The relative volumes of each phase in a fully phase-separated sample at triple coexistence are given by a two-dimensional analog of the lever rule [21]. For example, sample 5 in Fig. 5 is inside the triple triangle and just to the right of the middle of the gas-crystal edge (the edge connecting the gas and crystal phases), at $\phi \approx 0.37$. At equilibrium, it has only a small proportion of liquid phase, and roughly equal volumes of gas and crystal (see Fig. 10, rightmost image). Gas-liquid, liquid-crystal, and gas-crystal two-phase coexistence were observed just outside the triangular region of triple coexistence. These observations are consistent with

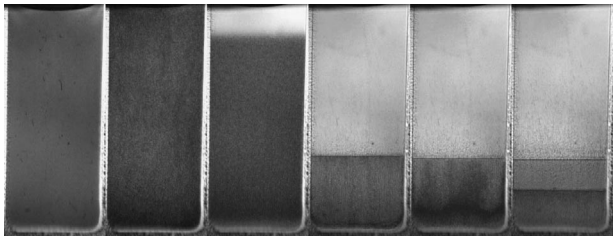

FIG. 6. Phase separation behavior of sample 1 after homogenization ($t=0$), frame numbering from left to right. Frame 1, $t=0$, homogeneous sample; 2, $t=2h15'$, the sample has increased turbidity (looks darker), presumably due to small droplets of the liquid and gas phases throughout the sample; 3, $t=5h30'$, droplets of the gas and liquid phases coalesce and are being gravitationally ordered to form a diffuse interface; 4, $t=16h15'$, metastable gas-liquid coexistence with a well-defined interface; 5, $t=21h15'$ nucleation of crystals throughout the liquid phase, visible as dark patches; 6, $t=42h15'$, the final equilibrium of the gas-liquid-crystal coexistence.

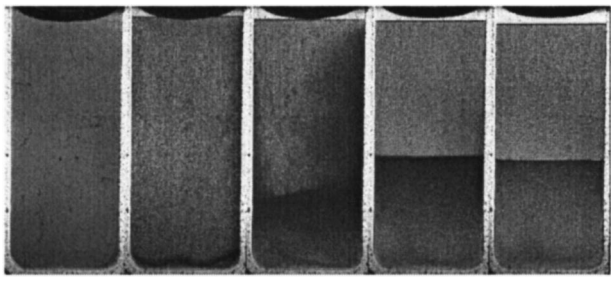

FIG. 7. Phase separation behavior of sample 2 after homogenization ($t=0$), frame numbering from left to right. Frame 1, $t=0$, homogenous sample; frame 2, $t=6h$, well-defined gas-liquid interface, with simultaneous nucleation of crystals (dense patches) in the denser, liquid phase; frame 3, $t=12h30'$, crystallites settle to form polycrystalline sediment, at the same time nucleation of both gas and crystallites is on-going; frame 4, $t=17h30'$, crystallization has ceased and liquid-crystal interface is now sharp. The amount of the gas phase has increased further; frame 5, $t=31h$, the crystalline phase has compacted slightly and is now in uniform, final three-phase equilibrium.

theory [8] and previous experiments on the same system at size ratios bracketing the value of $\xi=0.37$ used here [9].

At very high c_p, no macroscopically visible phase separation occurred during an initial period ranging from several hours for samples with low ϕ to days for samples with high ϕ, followed by a rapid formation of a dense sedimented phase and a very dilute supernatant phase. The dense phase was not iridescent initially, but a gradual buildup of iridescence starting from the bottom of the sample cell indicated crystallization within the sediment over a time of several weeks. This sequence of observations is consistent with the formation and subsequent collapse of a transient gel and resembles previous observations in colloid-polymer mixtures with a much lower size ratio of $\xi=0.08$ [9,22].

B. Kinetics of phase separation

In Sec. III we suggested that distinct kinetic regimes exist within the triple triangle where samples evolve toward gas, liquid, and crystal coexistence along different allowed pathways. In this section we report time-lapsed observations of samples labeled 1 to 6 in Fig. 5, and show that they indeed evolve towards three-phase coexistence along distinct kinetic pathways.

1. Sample 1

Figure 6 shows the behavior of sample 1. The turbidity increased very rapidly soon after homogenization (darkening of the sample: frame 1 to 2) and a diffuse interface formed soon thereafter (frame 3). This interface gradually moved down and became sharp soon after it stopped moving (frame 4). At this stage, only two phases could be distinguished, neither of which showed any iridescence. Soon thereafter, iridescent patches formed in the lower, denser phase (visible as dark patches in frame 5) and slowly settled to form a third phase (frame 6).

The early increase of turbidity indicative of large-scale density fluctuations, together with the observation (by eye) of a brightening and collapsing ring of intensity in small angle light scattering, suggests spinodal decomposition. The gravitational settling of a polydisperse population of (denser) liquid droplets produces a diffuse interface moving downwards. When this gas-liquid phase separation is complete, a sharp interface is formed. The liquid phase, however, is metastable with respect to liquid-crystal phase separation. The dark patches appearing throughout its volume (iridescent in incident light) are caused by small crystallites forming via homogenous nucleation. These fall under gravity and accumulate at the bottom of the sample cell. Careful observations confirm that the final liquid phase is slightly less turbid than the metastable liquid phase, suggesting that it is less concentrated. By the time the nucleation of crystals out of the liquid phase is complete, it is also possible to detect very small crystallites at the wall of the sample cell in the gas phase (though not visible in Fig. 6). This could be attributed to wall crystallization alone [23], but could also be indicative of crystal nucleation in the gas phase.

This observed sequence of events is consistent with regime *G* behavior already described in Sec. III. The position of sample 1 in the phase diagram is consistent with it following such a kinetic pathway [compare Fig. 5 with Fig. 2(c)]. Broadly similar behavior was also observed for sample 6: the detailed observations will therefore not be repeated.

2. Sample 2

The initial change in turbidity for sample 2, Fig. 7, is much less significant than for sample 1. Later (frame 2) a sharp interface appeared at the very top of the sample, separating a homogenous dilute phase (top) and a darker, denser phase. Throughout this dense phase, small dark patches could be seen that were iridescent to the eye and slowly settled to form a sediment. This phase separation process quickly became more vigorous (frame 3), then slowly decreased in rate again, and finally stopped (frame 4). Throughout this period, the upper interface continuously moved down, staying sharp all the time. Both top phases had a ho-

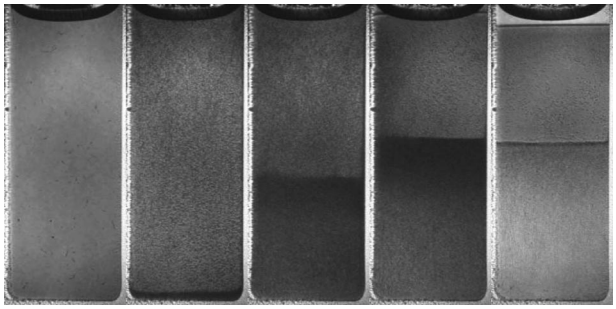

FIG. 8. Phase separation behavior of sample 3 after homogenization ($t=0$), frame numbering from left to right. Frame 1, $t=0$, homogeneous sample; frame 2, $t=4h45'$, nucleation of crystallites, visible as dark patches, throughout the sample with crystalline sediment starting to form; frame 3, $t=8h30'$, maximum crystallization and the diffuse crystal-liquid interface rising; frame 4, $t=12h$, crystallization almost ceased, the first gas-liquid interface visible at the very top; frame 5, $t=52h$, final equilibrium.

mogenous appearance, while the bottom phase appeared darker near its top. In the final three-phase equilibrium state, the bottom phase had compacted slightly and appeared homogenous.

The early sequence of observations suggests that both gas-liquid and liquid-crystal phase separation happen at the same time. A strong vertical flow pattern discernible in the video sequence soon after homogenization could be caused by droplets of both gas and crystalline nuclei rising and settling, respectively. The much slower initial increase in turbidity compared to sample 1 suggests that the mechanism of the gas-liquid phase separation is nucleation rather than spinodal decomposition. Again, some wall crystals were observed in the final gas phase.

The behavior observed corresponds to that briefly described for the kinetic regime *I* in Sec. III. The location of sample 2, Fig. 5, towards the liquid corner of the triple triangle, is consistent with where we expect to see regime *I* behavior, Figs. 2(a) and 2(b).

3. Sample 3

In sample 3 we observe no upper interface in the early stages, frame 2, Fig. 8, while dark patches (iridescent to the naked eye) were visible throughout the sample. A dilute phase appeared only very much later (top corners of frame 4), shortly before the formation of the bottom phase had finished, and most of it only formed later. These observations indicate that the liquid-crystal phase separation occurs first, and gas-liquid phase separation does not take place until after much of the first process has been completed. This is the behavior described for kinetic regime *J* in Sec. III. The position of this sample, Fig. 5, along the liquid-crystal edge of the triple triangle but at higher colloid volume fraction than sample 2, is consistent with finding regime *J* behavior, Fig. 2(a).

4. Sample 4

Figure 9 illustrates the behavior found for sample 4. The turbidity increased slowly at first. Then a sharp interface

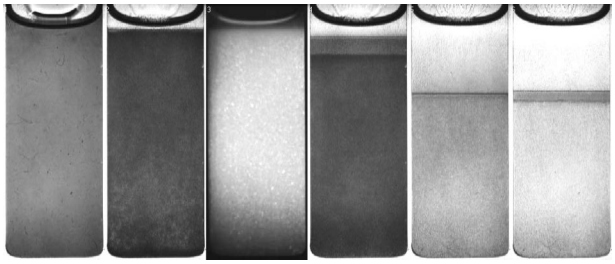

FIG. 9. Phase separation behavior of sample 4 after homogenization ($t=0$), frame numbering from left to right. Frame 1, $t=0$, homogenous sample; frames 2 and 3, $t=4h$, the dilute gas phase appears at the top and simultaneously throughout the denser phase, in frame 3 the illumination is adjusted to show the iridescent crystallites; frame 4, $t=7h$, crystallites have settled and there are well-defined gas-liquid and gas-crystal interfaces; frame 5, $t=23h$, the gas-liquid interface has become extremely diffuse and the crystalline phase has shrunk in volume; frame 6, $t=60h$, the final coexistence of gas, liquid, and crystal.

formed near the top of the sample, separating a dark dense phase and a homogenous, bright dilute phase (frame 2). In reflected light, small very bright patches that appeared iridescent to the naked eye could be seen in the dense phase (frame 3). As these gradually settled, a new sharp interface formed inside the dense phase, while the dilute phase on top continued to grow. The upper interface started to be slightly diffuse (frame 4) and subsequently became completely smeared out, while the lower interface continued to move down (frame 5). After the lower interface stopped moving, the upper interface reappeared. The amount of the middle phase was much reduced at final equilibrium (frame 6).

The early observations can be attributed to simultaneous nucleation of gas and crystals. As the crystals settled down under gravity, a second interface was formed between the crystalline phase and the remaining liquid. To find out more about the observed decrease in volume of the crystalline

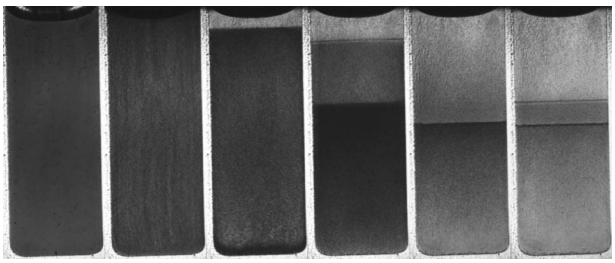

FIG. 10. Phase separation behavior of sample 5 after homogenization ($t=0$), frame numbering from left to right. Frame 1, $t=0$, homogenous sample; frame 2, $t=50'$, sample coarsened, vertical flow pattern has developed; frame 3, $t=4h$, gas phase at the top and crystallization and sedimentation of crystallites in the liquid phase (visible as dark patches and dark sediment); $t=8h50'$, crystallization has finished, the amount of gas phase has increased, both interfaces are well defined; frame 5, $t=20h10'$, the gas-liquid interface is extremely diffuse and the crystalline phase has decreased in volume; frame 6, $t=42h10'$, the gas-liquid interface has reappeared, and the final coexistence of colloidal gas, liquid, and crystal.

phase, static light scattering was performed. We found virtually no change in the crystal lattice parameter throughout the entire process. A clue to the origins of the observed ''compression'' comes from the concomitant ''disappearance'' of the gas-liquid interface. We suggest that the initial iridescent phase is made up of crystallites coated by gas layers. Later these layers detached and rose to the top of the sample, simultaneously decreasing the volume of the iridescent phase and destroying the sharp gas-liquid interface. Careful time-lapsed observations did indeed reveal upward flow patterns. This pattern of events is consistent with kinetic regime *L* described in Sec. III.

Note that Fig. 2(b) shows that kinetic regions *I* and *L* lie to the left of the metastable continuation of the high density branch of the gas-liquid binodal, while kinetic region *J* lies to the right. The discussion of samples 2–4 therefore implies that the metastable gas-liquid binodal separates sample 3 from samples 2 and 4; reference to Fig. 5 shows that this inference is consistent with the observed phase diagram.

5. Sample 5

The observations for sample 5 are shown in Fig. 10. A vigorous, predominantly vertical flow pattern developed after a short time (frame 2) and the sample had a very coarse, grainy appearance. Later, an interface separating a dilute top phase and a dense phase developed. In the dense phase, dark patches (iridescent to the eye) could be seen, which settled and formed a dark sediment (frame 3). The upper interface moved gradually down and stayed sharp until the end of the crystallization process (frame 4). Subsequently, the height of the sediment decreased, while it gradually brightened from the bottom of the sample. The upper interface almost disappeared (frame 5) and then reappeared at a much lower position only after the compaction of the sediment was finished (frame 6).

At least at first sight these observations suggest that, like sample 4, this sample is showing regime *L* behavior—the ''compaction'' of the crystalline sediment and the ''disappearance'' of the gas-liquid interface at intermediate times being evidence for the existence of gas coatings in the crystalline sediment when it was first formed. It is possible, however, that sample 5 may in fact belong to kinetic regime *G* (which is to the immediate left of regime *L* on the phase diagram, Fig. 2). There are two clues that this may be the case. First, the vigorous flow pattern observed early on is indicative of very fast gas-liquid phase separation, which is consistent with spinodal decomposition—this can occur in regime *G* but not *L*.

A second clue comes from the significantly smaller degree of compaction of the crystalline sediment observed here (frames 4 and 6, Fig. 10: a 14% compression) compared to the case of sample 4 (frames 4 and 6, Fig. 9: a 23% compression). The significance of this observation is somewhat subtle. The initial free-energy landscape of sample 5 dictates that any crystallites nucleated at the early stages *must* have gas coatings, because a liquid-crystal common tangent does not exist. However, as the phase separation proceeds, μ_p continuously decreases. There will come a point when a liquid-crystal common tangent becomes possible. From this point onwards, ''bare'' crystallites are permitted. These considerations are as relevant for sample 4 as for sample 5. However, if the gas-liquid phase separation proceeds via nucleation in sample 4 but via spinodal decomposition in sample 5, then the lowering of μ_p should proceed very much faster in the latter. This will mean that the amount of gas-coated crystallites relative to bare crystallites in sample 5 should be significantly lower than in sample 4, thus explaining the smaller degree of compression observed. Note that in sample 1, which also belonged to kinetic regime *G*, the initial polymer chemical potential was sufficiently low that nucleation of bare crystallites was possible from the beginning, so that no compaction of the crystalline sediment was observed.

VI. CONCLUSIONS

We have presented time-lapse video evidence to show that within the triple triangle in the phase diagram of a colloid-polymer mixture, distinct kinetic regions exist in which phase separation into colloidal gas, liquid, and crystal phases follow different kinetic pathways. The existence of these kinetic regimes, as well as their location on the phase diagram, can be understood using a simple construction on the free-energy landscape of the system first enunciated by Cahn [10]. This approach shows that metastable minima in the free-energy landscape, while having no relevance for determining the equilibrium phase diagram, nevertheless can exercise decisive influence on the phase transition kinetics. Our analysis can therefore be seen as providing support for the well-known ''Ostwald step rule'' [24].

The approach illustrated here of using the free-energy landscape to turn phase diagrams into kinetic maps is general [6]. Thus, preliminary work suggests that it may also be fruitfully used to illuminate the kinetic behavior in multiphase surfactant systems [25]. In the companion paper [4] we present the theory underlying our data interpretation and numerics supporting the underlying assumptions.

ACKNOWLEDGMENTS

Our thanks goes to Dr. Laura Starrs for her key contribution to setting up the optical apparatus. This work was funded by EPSRC Grant No. GR/K56205.

[1] P. M. Chaikin and T. C. Lubensky, *Principles of Condensed Matter Physics* (Cambridge University Press, Cambridge, 1995).

[2] A. J. Bray, Adv. Phys. **43**, 357 (1994).

[3] *Soft and Fragile Matter: Non-equilibrium Dynamics, Metastability and Flow*, edited by M. E. Cates and M. R. Evans (Institute of Physics, Bristol, 2000).

[4] R. M. L. Evans, W. C. K. Poon, and F. Renth, Phys. Rev. E **64**,

031403 (2001).
[5] W. C. K. Poon *et al.*, Phys. Rev. Lett. **83**, 1239 (1999).
[6] W. C. K. Poon, F. Renth, and R. M. L. Evans, J. Phys.: Condens. Matter **23**, A269 (2000).
[7] S. Asakura and F. Oosawa, J. Chem. Phys. **22**, 1255 (1954).
[8] H. N. W. Lekkerkerker *et al.*, Europhys. Lett. **20**, 559 (1992).
[9] S. M. Ilett, A. Orrock, W. C. K. Poon, and P. N. Pusey, Phys. Rev. E **51**, 1344 (1995).
[10] J. W. Cahn, J. Am. Ceram. Soc. **52**, 118 (1969).
[11] L. Antl *et al.*, Colloids Surface **17**, 67 (1986).
[12] P. N. Pusey *et al.*, Phys. Rev. Lett. **63**, 2753 (1989).
[13] P. N. Pusey and W. van Megen, J. Chem. Phys. **80**, 3513 (1984).
[14] W. G. Hoover and F. H. Ree, J. Chem. Phys. **49**, 3609 (1968).
[15] S. E. Paulin and B. J. Ackerson, Phys. Rev. Lett. **64**, 2663 (1990).
[16] S. M. Underwood, J. R. Taylor, and W. van Megen, Langmuir **10**, 3550 (1994).
[17] W. Burchard, Adv. Polym. Sci. **48**, 1 (1983).
[18] C. G. Berry, J. Chem. Phys. **44**, 4550 (1966).
[19] P. J. Flory and S. Fisk, J. Chem. Phys. **44**, 2243 (1966).
[20] P. B. Warren, S. M. Ilett, and W. C. K. Poon, Phys. Rev. E **52**, 5205 (1995).
[21] R. T. DeHoff, *Thermodynamics in Materials Science* (McGraw-Hill, New York, 1993).
[22] W. C. K. Poon *et al.*, Faraday Discuss. **112**, 143 (1999).
[23] A. D. Dinsmore, P. B. Warren, W. C. K. Poon, and A. G. Yodh, Europhys. Lett. **40**, 337 (1997).
[24] W. Ostwald, Z. Phys. Chem., Stoechiom. Verwandtschaftsl. **22**, 289 (1897).
[25] M. Buchanan, L. Starrs, S. U. Egelhaaf, and M. E. Cates, Phys. Rev. E **62**, 6895 (2000).